Journal of Solid State Chemistry **164,** 220–229 (2002)
doi:10.1006/jssc.2001.9463, available online at http://www.idealibrary.com on IDEAL®

Sr_3NiRhO_6 and Sr_3CuRhO_6—Two New One-Dimensional Oxides. Magnetic Behavior as a Function of Structure: Commensurate vs Incommensurate

K. E. Stitzer, W. H. Henley, J. B. Claridge,[1] and H.-C. zur Loye[2]

Department of Chemistry and Biochemistry, University of South Carolina, Columbia, South Carolina, 29208

and

R. C. Layland

Division of Biological and Physical Sciences, Lander University, Greenwood, South Carolina, 29649

Received August 17, 2001; in revised form November 2, 2001; accepted November 16, 2001; published online February 12, 2002

Two new compounds, Sr_3NiRhO_6 and Sr_3CuRhO_6, belonging to a family of 2H-perovskite related materials, were synthesized in both a commensurate and an incommensurate form. The oxides were structurally characterized by powder X-ray Rietveld refinements and magnetic measurements. The commensurate structure of Sr_3NiRhO_6 is isostructural with the rhombohedral K_4CdCl_6 structure (space group $R\bar{3}c$; $Z = 6$; $a = 9.5951(1)$ Å, $c = 11.0621(2)$ Å) while the structure of Sr_3CuRhO_6 forms in a monoclinic distortion of the K_4CdCl_6 structure (space group $C\,2/c$; $Z = 4$; $a = 9.2226(2)$ Å, $b = 6.9882(2)$ Å, $c = 6.6926(2)$ Å, $\beta = 92.440(2)^\circ$). The structures of Sr_3NiRhO_6 and Sr_3CuRhO_6 contain chains of alternating face-sharing NiO_6/CuO_6 trigonal prisms and RhO_6 octahedra. The magnetic susceptibility of Sr_3NiRhO_6 shows an abrupt drop at 30 K, suggesting antiferromagnetic correlations between the transition metal containing chains. Sr_3CuRhO_6 displays ferromagnetic-type ordering below 10 K. When the samples are heated for prolonged periods of time, a transition to an incommensurate structure takes place. Depending on the specific synthesis conditions, different incommensurate structures can be obtained. The fitted lattice parameters with space group $R3m$ (cell 1) and $P31c$ (cell 2) are $a = 9.6201(6)$ Å, $c_1 = 2.6732(2)$ Å, $c_2 = 3.9803(8)$ Å for $Sr_3NiRhO_{6+\delta}$ and $a = 9.624(2)$ Å, $c_1 = 2.6981(5)$ Å, $c_2 = 3.9539(5)$ Å for $Sr_3CuRhO_{6+\delta}$. The magnetic susceptibilities of the incommensurate compounds are quite different from their commensurate analogues, as all signs of long-range magnetic order disappear.

Key Words: **Sr_3NiRhO_6; Sr_3CuRhO_6; solid-state synthesis; oxides; Rietveld refinement; commensurate structures; incommensurate structures; magnetic properties.**

INTRODUCTION

We have previously reported the crystal structures of several 2H-perovskite related oxide materials, including Sr_3ZnRhO_6 (1), Sr_3GdRhO_6 (2), Sr_3ScRhO_6 (3), Ca_3NaMO_6 (M = Ru, Ir) (4), Sr_3CoPtO_6 (5), Sr_3PbNiO_6 (6), and $Sr_6Rh_5O_{15}$ (7,8). These phases belong to a large family of oxide structures and can be described via the stacking of $[A_3O_9]$ and $[A_3A'O_6]$ layers, and the filling of the resultant octahedral interstices by a B cation (9). This gives rise to the general expression $A_{3n+3m}A'_nB_{3m+n}O_{9m+6n}$ (10,11). Using this formalism, compounds such as $Sr_6Rh_5O_{15}$ correspond to an $m = 1$, $n = 1$ structure (A = Sr; $A' = B$ = Rh), while Sr_3PbNiO_6 represents the $m = 0$, $n = 1$ member, as shown in Fig. 1. This description easily describes the structural composition of the commensurate members but not as readily the members that form an incommensurately modulated structure.

An alternative method for describing these structures is to treat them as composite crystals in terms of two subcells (11–15). The first subcell consists of $[(A', B)O_3]_\infty$ chains while the second is formed by the $[A]_\infty$ chains; these are two crystallographically independent subsystems that are periodic in the xy plane and modulated along the z direction. If the ratio of the repeat distances of these two chain types is a rational number, then the structure is commensurate; however, if the ratio is not a rational number, then the structure is incommensurately modulated along the chain direction.

An equivalent expression for this family of oxides is $A_{1+x}(A'_xB_{1-x})O_3$ ($x = n/(3m + 2n)$) where the composition variable x ranges continuously between 0 and $\frac{1}{2}$ (13). For simple fractional values of x, such as $\frac{1}{5}$, $\frac{2}{7}$, or $\frac{1}{3}$, the structure

[1]Current address: Department of Chemistry, University of Liverpool, Crown Street, Liverpool L69 7ZD, UK.

[2]To whom correspondence should be addressed. E-mail: zurloye@sc.edu.

0022-4596/02 $35.00

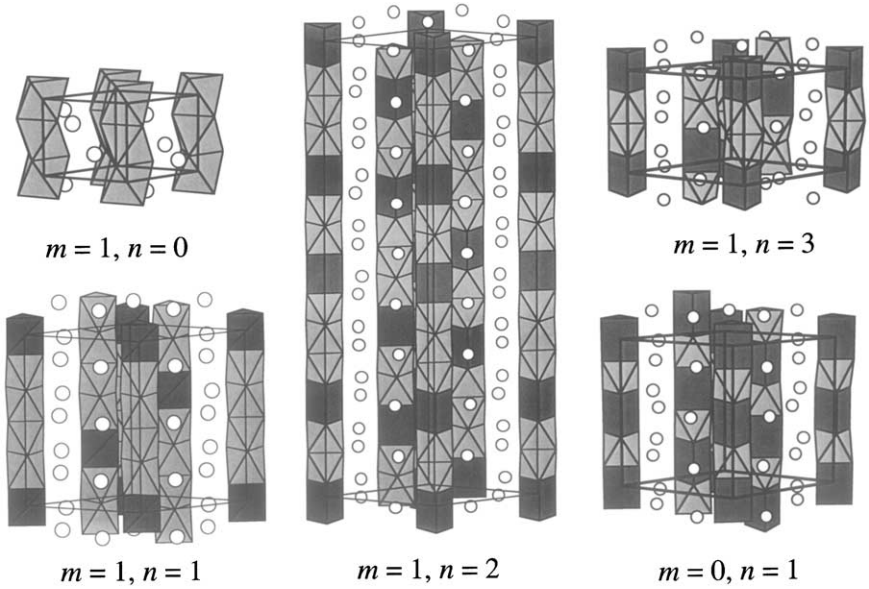

FIG. 1. Structures of the $A_{3n+3}A'_nB_{n+3}O_{6n+9}$ family.

is commensurate. Numerous incommensurate members of this family have also been found (14,16–18) and the usefulness of this structural model has been demonstrated by such incommensurate structures as $Ba_{1+x}[(Cu_xRh_{1-x})O_3]$ with $x = 0.1605$ and $x = 0.1695$ (12), and $Ba_{1+x}[(Cu_xIr_{1-x})O_3]$ with $x = 0.2708$ (19).

The $m = 0$, $n = 1$ members of this family form in the familiar K_4CdCl_6 structure and are of the type $A_3A'BO_6$ consisting of infinite chains of face-shared $A'O_6$ trigonal prisms and BO_6 octahedra. The A' and B sites can be occupied by diverse cations in oxidation states ranging from $+1$ to $+5$. When both the A' and the B site are occupied by magnetic ions, complex magnetic interactions within chains can be observed. If, on the other hand, only one site (either A' or B) contains a magnetic ion, coupling between chains can dominate (20, 21). In addition, since six other chains surround each chain, forming a triangular lattice in the basal plane, such systems can be expected to exhibit spin glass behavior or geometric frustration (22).

There is now a growing number of compounds with the K_4CdCl_6 structure that contain magnetic ions on both the A' and the B chain sites: Ca_3CoIrO_6 (23), Ca_3CoRuO_6 (24), Sr_3CoPtO_6 (5), Ca_3NiMnO_6 (24), Sr_3NiIrO_6 (25), Sr_3CuIrO_6, (25), Ca_3CoRhO_6 (26), Ca_3FeRhO_6 (26), and $Ca_3Co_2O_6$ (27–32). These materials have all been shown to exhibit very complex magnetic behavior due to interactions both within and between chains. For some compounds, such as $Ca_3Co_2O_6$, low-temperature neutron diffraction has yielded insights into the magnetic structure of these materials (30, 31). In others, such as Sr_3NiIrO_6, no magnetic Bragg peaks were observed down to the lowest temperatures measured (25).

In this paper we report the synthesis of Sr_3NiRhO_6 and Sr_3CuRhO_6, two new $m = 0$, $n = 1$ members of this family of oxides, that can be synthesized in the K_4CdCl_6 structure as well as in incommensurate modifications. The complex magnetic properties of these two compounds, measured for both the commensurate and the incommensurate modifications, are reported and compared with the magnetic properties of the known iridium analogues, Sr_3NiIrO_6 and Sr_3CuIrO_6.

EXPERIMENTAL

Synthesis

Polycrystalline samples of Sr_3NiRhO_6 and Sr_3CuRhO_6 were synthesized *via* a solid state route. $SrCO_3$ (Alfa, 99.95%), NiO or CuO (Alfa, 99.95%), and Rh metal (Engelhard, 99.9995%), were intimately mixed and ground thoroughly. The powder was pressed into a pellet at 5000 psi and heated at 1000°C for a total of 15 days with intermittent grinding. To prepare the commensurate phases, great care had to be taken not to heat the samples too long, as the transformation to the incommensurate phase, although slow, starts as soon as the commensurate target phase has formed. Due to this circumstance, a small amount of the incommensurate phase is always found in the commensurate phases of both Sr_3NiRhO_6 and Sr_3CuRhO_6.

Further heat treatments of the commensurate samples lead to incommensurate phases. However, in order to synthesize phase pure incommensurate samples, a nitrate

decomposition was employed. $SrCO_3$ (Alfa, 99.95%), NiO or CuO (Alfa, 99.95%), and Rh metal (Engelhard, 99.9995%) were intimately mixed and ground thoroughly. The powder was dissolved in 250 mL of concentrated nitric acid. The reaction mixture was heated and stirred until dryness. The dried reaction mixture was initially heated in air at 400°C for 20 h. It was then fired at 850°C for 12 h, 1000°C for 72 h, 3 cycles of 1050°C for 72 h, and a final treatment at 1150°C for 88 h.

Structure Refinement

High-resolution synchrotron X-ray powder diffraction data were collected on the X7A beamline at the National Synchrotron Light Source at Brookhaven National Laboratory. Monochromatic radiation was obtained from a channel-cut double-crystal Si (111) monochromator, oriented to give a wavelength of 0.7997(1) Å. The synchrotron wavelength was calibrated using a CeO_2 standard. The samples were loaded into glass capillaries (diameter $\sim$ 0.2 mm), which were freely rotated (1–2 Hz) during data collection to reduce any possible preferred orientation effects. Data collection times were typically 4 h per sample.

Structure refinements of Sr_3NiRhO_6 were carried out in the space group $R\bar{3}c$ (no. 167). Based on our experience with the structure of Sr_3NiPtO_6 (20,33), the Rh atom was placed in the octahedral site 6*b*, the Ni atom was placed in the trigonal prismatic site 6*a*, and the Sr atom was placed in the 18*e* site. The structure refinement of Sr_3CuRhO_6 was carried out in the space group *C* 2/*c* (no. 15). Using the known structure of Sr_3CuPtO_6 as a starting point (34), the Rh atom was placed in the octahedral site 4*c*, the Cu atom was placed in the trigonal prismatic site 4*e*, and the Sr atom was placed in the 4*e* and 8*f* sites.

Structure refinements for both compounds were performed using the Rietveld (35) method implemented in the computer program GSAS (36). The profile of the diffraction peaks of Sr_3NiRhO_6 and Sr_3CuRhO_6 was described by a pseudo-Voigt function. Refinements of the peak asymmetry were allowed and a linear interpolation of fixed points was used to model the background.

Magnetism

The magnetic susceptibilities of the polycrystalline samples were measured using a Quantum Design MPMS XL SQUID magnetometer. Samples were measured under both field cooled (FC) and zero-field-cooled (ZFC) conditions. In either case, the magnetization was measured upon warming the samples from 2 to 300 K. Susceptibility measurements were carried out in applied fields of 500, 1000, 5000, and 40,000 G. In addition, field sweeps between + 40,000 and − 40,000 G were measured at various temperatures. The very small diamagnetic contribution of the gelatin capsule containing the sample had a negligible contribution to the overall magnetization, which was dominated by the sample.

Thermogravimetric Analysis

The oxygen content of the samples and their thermal behavior was determined by thermogravimetric analyses (TGA), using a TA Instruments SDT 2960 simultaneous DTA-TGA. Thermogravimetric analyses used 5% H_2/95% N_2 (flow rate of 60 mL/min). Analyses of the oxygen content were carried out on both commensurate and incommensurate samples of Sr_3NiRhO_6 and Sr_3CuRhO_6. To carry out the reductions, samples of Sr_3NiRhO_6 and Sr_3CuRhO_6 were heated over a temperature range of 50 to 1100°C at a heating rate of 5°C/min. The oxygen content was determined based on the weight loss and the oxygen content of the residual species (strontium oxide, nickel/copper metal, and rhodium metal). The endpoint of the TGA trace was not always well defined, leading to a larger than normal uncertainty in the oxygen content of these materials.

RESULTS

Commensurate Structures

Crystallographic data for the structure refinements of Sr_3NiRhO_6 and Sr_3CuRhO_6 are given in Table 1. The atomic positions and thermal parameters for Sr_3NiRhO_6 and Sr_3CuRhO_6 can be found in Table 2. Selected interatomic distances and angles for the nickel and copper phases are located in Tables 3 and 4, respectively. The best agreement obtained between the calculated and the observed profiles for the Rietveld refinement of Sr_3NiRhO_6 and Sr_3CuRhO_6 is shown in Figs. 2 and 3, respectively. Due to the fact that a small amount of the respective incommensurate phase was present in both powder diffraction patterns, it was not possible to refine these structures to very low residuals. Using the current software it is not possible to

TABLE 1
Summary of Crystallographic Data and Least-Squares Refinement Results for Sr_3MRhO_6 (M = Ni and Cu)

Compound	Sr_3NiRhO_6	Sr_3CuRhO_6
Space group	$R\bar{3}c$	$C2/c$
a (Å)	9.5951(1)	9.2226(2)
b (Å)	9.5951(1)	9.6882(2)
c (Å)	11.0621(2)	6.6926(2)
α (°)	90	90
β (°)	90	92.440(2)
γ (°)	120	90
V (Å^3)	882.00(3)	597.45(3)
R_p (%)	11.16	10.08
R_{wp} (%)	12.64	10.44
R_{Bragg} (%)	9.13	9.26

TABLE 2
Atomic Positions and Isotropic Thermal Parameters with ESDS ( ) for Sr_3MRhO_6 (M = Ni and Cu)

Compound	Atom	Site	x	y	z	U_{iso} (Å^2)
Sr_3NiRhO_6	Rh	6*b*	0	0	0	0.0067(4)
	Sr	18*e*	0.3653(1)	0	$\frac{1}{4}$	0.0080(3)
	Ni	6*a*	0	0	$\frac{1}{4}$	0.0062(6)
	O	36*f*	0.1721(6)	0.0221(7)	0.1119(5)	0.012(1)
Sr_3CuRhO_6	Rh	4*c*	$\frac{1}{4}$	$\frac{1}{4}$	0	0.0043(4)
	Sr	8*f*	0.3128(2)	0.0737(2)	0.6195(4)	0.0063(5)
	Sr	4*e*	0	0.1064(3)	$\frac{1}{4}$	0.010(8)
	Cu	4*e*	$\frac{1}{2}$	0.1987(3)	$\frac{1}{4}$	0.0020(7)
	O[a]	8*f*	0.217(1)	0.312(1)	0.7154(7)	0.01
	O[a]	8*f*	0.360(1)	0.4237(7)	0.073(2)	0.01
	O[a]	8*f*	0.0555(6)	0.340(1)	0.030(2)	0.01

[a]Oxygen positions have been constrained. Oxygen thermal parameters are fixed.

TABLE 4
Select Interatomic Distances (Å) and Bond Angles (°) with ESDS ( ) for Sr_3CuRhO_6

Atom	Atom	Distance		Atom	Atom	Atom	Angle	
Rh	Cu	2.8344(6)	(×2)	O(1)	Rh	O(2)	92.1(5)	(×2)
Rh	O(1)	2.009(2)	(×2)	O(1)	Rh	O(2)	87.9(5)	(×2)
Rh	O(2)	2.014(2)	(×2)	O(1)	Rh	O(3)	82.2(5)	(×2)
Rh	O(3)	2.011(2)	(×2)	O(1)	Rh	O(3)	97.8(5)	(×2)
Cu	O(1)	2.02(1)	(×2)	O(2)	Rh	O(3)	93.2(5)	(×2)
Cu	O(2)	2.77(1)	(×2)	O(2)	Rh	O(3)	86.8(5)	(×2)
Cu	O(3)	1.96(1)	(×2)	O(1)	Cu	O(2)	174.0(6)	
				O(1)	Cu	O(3)	83.2(3)	
				O(1)	Cu	O(3)	95.7(2)	
				O(2)	Cu	O(3)	95.7(2)	
				O(2)	Cu	O(3)	83.1(6)	
				O(3)	Cu	O(3)	158.1(7)	

carry out a two-phase Rietveld refinement with an incommensurate structure. Consequently, no corrections of any sort were carried out to compensate for the presence of the incommensurate component. The residuals, therefore, for Sr_3NiRhO_6 were $R_p = 11.16\%$ and $R_{wp} = 12.64\%$ and for Sr_3CuRhO_6 $R_p = 10.08\%$ and $R_{wp} = 10.44\%$.

Sr_3NiRhO_6 is isostructural with the rhombohedral structure type K_4CdCl_6, as was expected based on the fairly large number of compounds that have been synthesized with this structure type. Sr_3CuRhO_6 forms in a monoclinic distortion of the K_4CdCl_6 structure type (34). The rhombohedral structure consists of chains of alternating face-sharing trigonal prisms and octahedra. In the monoclinic modification, the copper atoms move from the center of the trigonal prisms to their faces, thereby taking on a pseudo-square planar coordination. A comparison between the two types of chains is shown in Fig. 4. The strontium ions are coordinated in a distorted square antiprism by eight oxygens. The rhodium ions are located at the corners and center of the unit cell and are octahedrally coordinated to six oxygens. The Rh–O bond distances are in agreement with those found for Rh(IV) in other structurally related oxides (1,7,37). The nickel ions in Sr_3NiRhO_6 are located at the corners and center of the unit cell and are coordinated in a trigonal prismatic array by six equivalent oxygens. The trigonal prisms are distorted by a twist about the threefold axis (ϕ) of 13.6°. The copper ions in Sr_3CuRhO_6 are also located at the corners and the center of the unit cell and are coordinated in a trigonal prismatic array by 6 nonequivalent oxygens. Due to the preference for copper to be in a square planar

TABLE 3
Select Interatomic Distances (Å) and Bond Angles (°) with ESDS ( ) for Sr_3NiRhO_6

Atom	Atom	Distance		Atom	Atom	Atom	Angle	
Rh	Ni	2.76552(6)	(×2)	O	Rh	O	94.7(2)	(×6)
Rh	O	1.989(5)	(×6)	O	Rh	O	85.4(2)	(×6)
Ni	O	2.181(5)	(×6)	O	Rh	O	180	(×3)
				O	Ni	O	76.4(2)	(×6)
				O	Ni	O	89.7(3)	(×3)
				O	Ni	O	129.4(3)	(×3)
				O	Ni	O	147.3(3)	(×3)

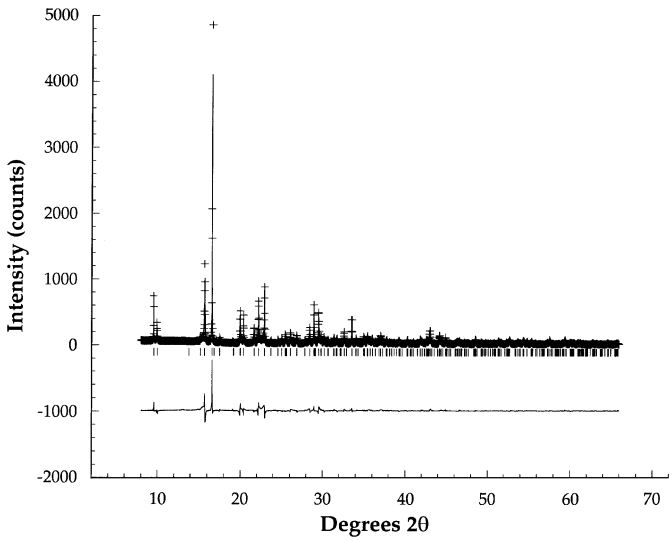

FIG. 2. Observed (cross) and calculated (solid line) X-ray diffraction patterns of Sr_3NiRhO_6 for the range 8°–66° 2θ, where $\lambda = 0.79970$ Å, corresponding to d-spacings of 5.732–0.734 Å. Tick marks indicate the positions of allowed Bragg reflections. The difference line, observed minus calculated, is located at the bottom of the figure.

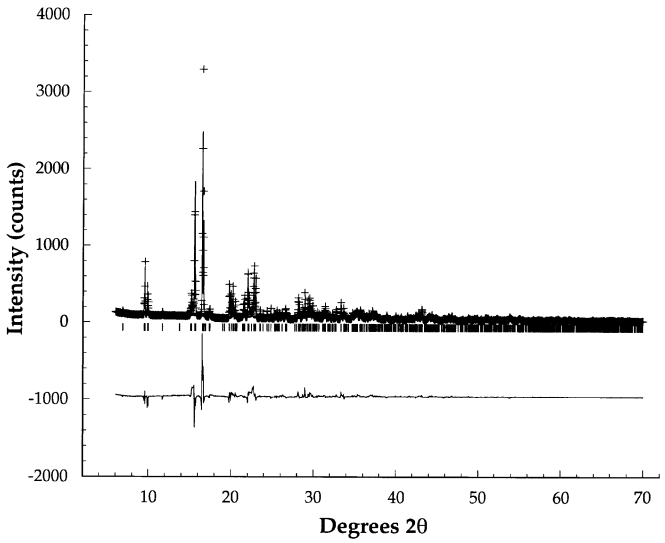

FIG. 3. Observed (cross) and calculated (solid line) X-ray diffraction patterns of Sr_3CuRhO_6 for the range 6°–70° 2θ, where $\lambda = 0.79970$ Å, corresponding to d-spacings of 7.640–0.697 Å. Tick marks indicate the positions of allowed Bragg reflections. The difference line, observed minus calculated, is located at the bottom of the figure.

coordination environment, the copper atoms move from the center of the trigonal prism to one of the faces, thereby achieving a pseudo square planar arrangement, leading to four short and two long Cu–O distances. An approximate [110] view of the $m = 0$, $n = 1$ structure type is shown in Fig. 1, showing the alternating repeat of one octahedron and one trigonal prism along the c direction for both Sr_3NiRhO_6 and Sr_3CuRhO_6.

Incommensurate Structures

The powder X-ray diffraction pattern for $Sr_3NiRhO_{6+\delta}$ and $Sr_3CuRhO_{6+\delta}$ are shown in Figs. 5 and 6, respectively. They cannot be indexed using a conventional 3D cell; however, the patterns can be fully indexed using four indices ($hklm$), implementing a similar method as shown for other incommensurate compounds (1, 15, 18). The $[(M, \mathrm{Rh})O_3]_\infty$ subsystem was chosen as the reference subsystem. The reflections belonging to the two subcells are marked by the upper set of tick marks beneath each pattern ($hkl0$, $hk0m$), while the lower set of tick marks correspond to reflections attributable to the modulation ($hklm$). The fitted lattice parameters with space groups $R3m$ (subsystem 1) and $P31c$ (subsystem 2) are $a = 9.6201(6)$ Å, $c_1 = 2.6732(2)$ Å, $c_2 = 3.9803(8)$ Å for $Sr_3NiRhO_{6+\delta}$ and $a = 9.624(2)$ Å, $c_1 = 2.6981(5)$ Å, $c_2 = 3.9539(5)$ Å for $Sr_3CuRhO_{6+\delta}$. The c_1/c_2 ratio, which is indicative of the ratio of layers in the structure to polyhedra in the transition metal chain, are

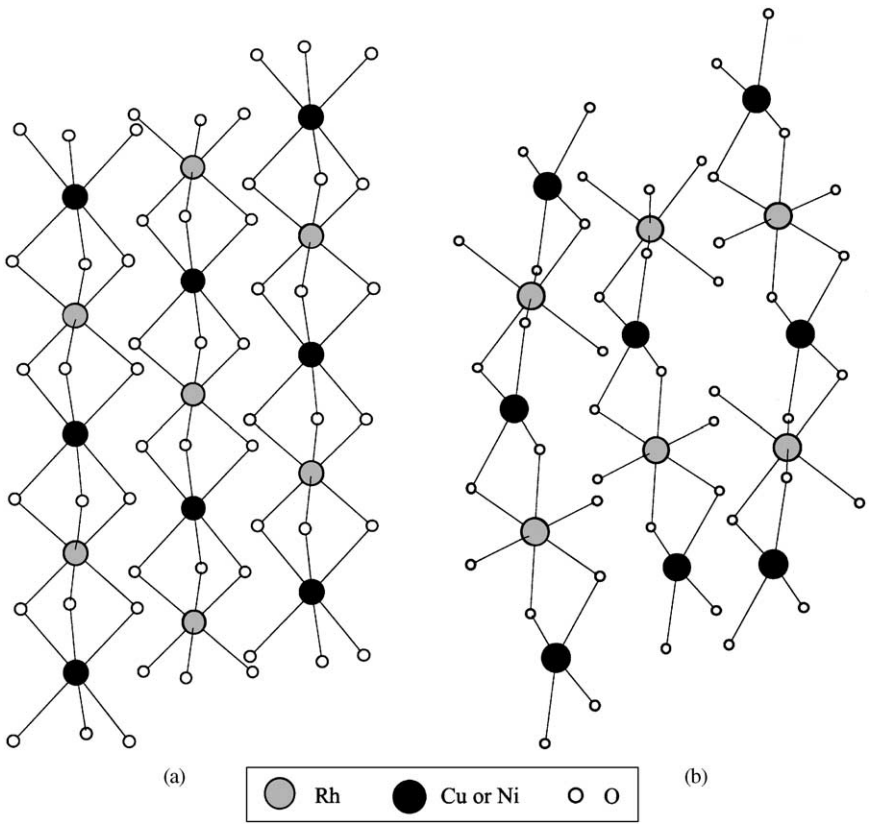

FIG. 4. Comparison of the $[A'RhO_6]_\infty$ chains in Sr_3NiRhO_6 (a) and Sr_3CuRhO_6 (b).

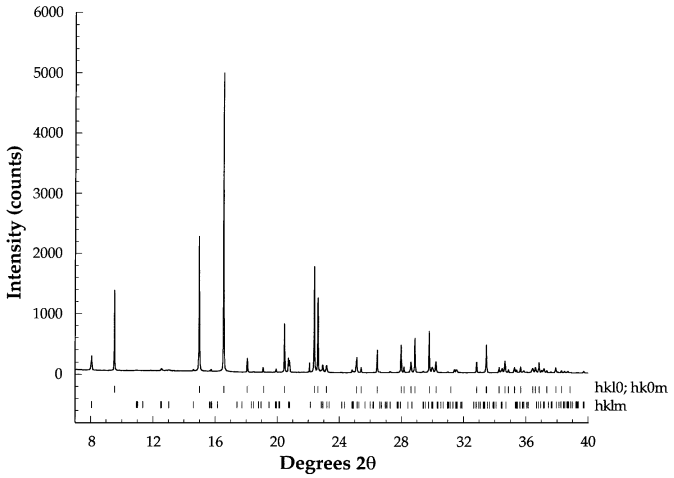

FIG. 5. Diffraction pattern for the incommensurate form of $Sr_3NiRhO_{6+\delta}$ for the range 8°–40° 2θ, for $\lambda = 0.79970$ Å, corresponding to *d*-spacings of 5.732–1.169 Å. The reflections belonging to the two subcells are marked by the upper set of tick marks beneath each pattern (*hkl*0, *hk*0*m*), while the lower set of tick marks correspond to reflections attributable to the modulation (*hklm*).

0.6716 and 0.6824, for the nickel and the copper compounds, respectively, compared to a theoretical value for the commensurate $m = 0$, $n = 1$ structure of 0.75. A smaller experimental c_1/c_2 value compared to the theoretical value indicates that some of the trigonal prisms have been converted to octahedra and that the structure no longer strictly contains alternating octahedra and trigonal prisms along the polyhedral chain. In fact, a value of 0.67 corresponds to a structure having, on average, two octahedra for every trigonal prism.

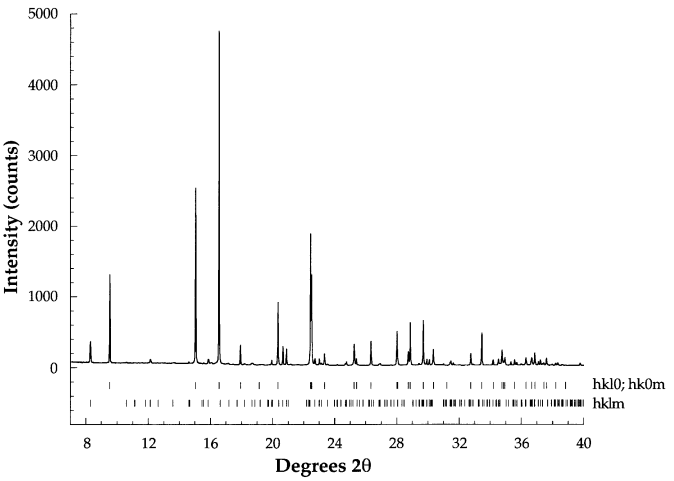

FIG. 6. Diffraction pattern for the incommensurate form of $Sr_3CuRhO_{6+\delta}$ for the range 8°–40° 2θ, for $\lambda = 0.79970$ Å, corresponding to *d*-spacings of 5.732–1.169 Å. The reflections belonging to the two subcells are marked by the upper set of tick marks beneath each pattern (*hkl*0, *hk*0*m*), while the lower set of tick marks correspond to reflections attributable to the modulation (*hklm*).

Thermogravimetric Analysis

The oxygen content of the four phases was determined by TGA. The samples were reduced in flowing hydrogen to the metals plus SrO, and the oxygen content was determined based on the weight loss. The oxygen content for the commensurate phases was stoichiometric within experimental error. The oxygen content for the two incommensurate phases, however, was higher than that predicted for the commensurate $m = 0$, $n = 1$ structure. The increased oxygen content indicates an overall oxidation of the incommensurate phase relative to the commensurate one. The results are only qualitative and not quantitative in nature, since a reasonable endpoint was not observed. Other members of this family have also displayed such a poorly defined endpoint in the TGA data (18, 38). Qualitatively, the weight loss for the nickel phase was 10.0%, corresponding to an oxygen content of 6.3, and 9.9% for the copper phase, corresponding to an oxygen content of 6.3.

Magnetic Measurements

The magnetic susceptibility data for the commensurate Sr_3NiRhO_6 phase was measured at 5 kG and is shown in Fig. 7. (The data obtained at 1 and 2.5 kG are qualitatively identical and are not shown for clarity.) Above 100 K (not shown) the susceptibility of both the ZFC and FC data follow the Curie–Weiss Law. Fitting the high-temperature data to the Curie–Weiss Law plus a temperature-independent term (TIP), according to the equation $\chi = C/(T - \theta) + \text{TIP}$ (18), yields a calculated effective moment of 2.61 μ_B, ($\theta = 28.3$ K; TIP = 0.00138 emu/mol), which is lower than the theoretical spin-only moment of 3.31 μ_B for Rh^{4+} in the octahedral site and Ni^{2+} in the trigonal prismatic site. A lower than expected effective moment has also been observed for other members of this family (38). At low temperatures, the ZFC susceptibility shows a sharp drop around 15 K, which levels off near 10 K. The susceptibility data measured in different applied fields overlay reasonably well, indicating that there is virtually no field dependence to the measurement. The FC measurements, on the other hand, do not show this sharp drop at 15 K, but rather the susceptibility continues to increase until about 10 K, when it levels off at a value much higher than that for the ZFC data. Again, there is little if any field dependence for the FC measurements.

The susceptibility data look very similar to what has been observed for other members of this family, such as Ca_3FeRhO_6 (26), Ca_3CoRhO_6 (26), and Sr_3NiIrO_6 (25). While the susceptibility of the iridium compound displays the sharp drop at a temperature slightly higher than that of

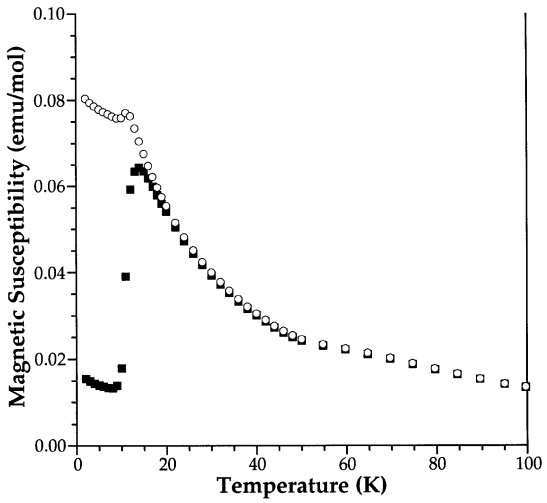

FIG. 7. Temperature dependence of the ZFC (■) and FC (○) magnetic susceptibility measured at 5 kG for Sr_3NiRhO_6.

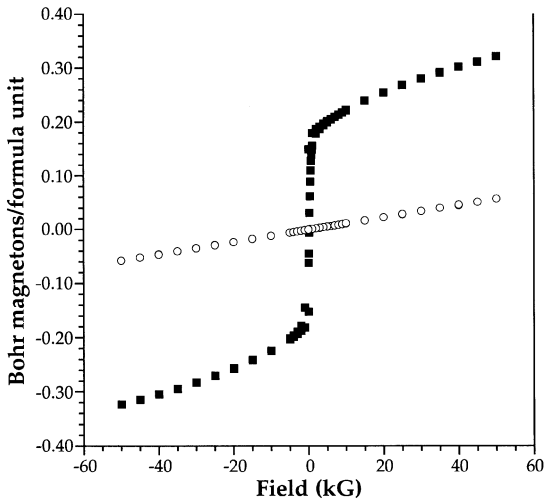

FIG. 9. Field dependence of the magnetization of Sr_3CuRhO_6 measured at 3 (■) and 70 K (○).

the rhodium phase, the overall shape of the susceptibility data is strikingly similar, and in fact, equally similar to that of Ca_3FeRhO_6 and Ca_3CoRhO_6. Although the magnetic transition in the susceptibility of Sr_3NiRhO_6 is very intense, field sweeps collected at 3 and 70 K, below and above the susceptibility drop, respectively, were linear and did not show any field dependence.

The magnetic susceptibility of Sr_3CuRhO_6 was measured in applied fields of 0.5, 5, and 40 kG. The 500-G measurement is shown in Fig. 8. The data follow Curie–Weiss type behavior at temperatures above 75 K. Fitting the high-temperature data to the Curie–Weiss Law plus TIP yields a calculated effective moment of 1.57 μ_B ($\theta = 11.2$ K; TIP = 0.00118 emu/mol), which is also lower than the theoretical spin-only moment for Rh^{4+} in an octahedral coordination and Cu^{2+} in a square planar coordination of 2.45 μ_B. The data are consistent with a ferromagnetic-type ordering below 10 K. At high fields, both ZFC and FC data overlay down to the lowest temperature measured, 2 K. Only at very low applied fields (500 G or less), as shown, is there a clear separation between the ZFC and FC data collected. Whereas the FC data appear to be ordering ferromagnetically, the ZFC data undergo a second transition and below 5 K tend toward zero. Such deviations between the ZFC and the FC data are often indicative of geometric frustration or a spin glass state, which is possible in these materials due to their quasi-triangular structure.

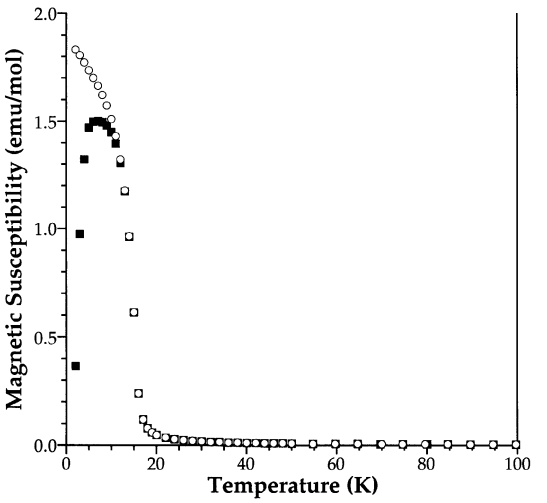

FIG. 8. Temperature dependence of the ZFC (■) and FC (○) magnetic susceptibility measured at 500 G for Sr_3CuRhO_6.

The field dependence of the magnetization, shown in Fig. 9, indicates that at 3 K, Sr_3CuRhO_6 looks like a very soft ferromagnet. In fact, there is virtually no observable hysteresis. A careful analysis of the data, however, reveals that below about 500 G, there is a small hysteretic loop. Based on the data shown in Fig. 9, it is unlikely, however, that this represents the type of hysteresis observed for normal ferromagnetic materials. The *M* vs H curve measured at 70 K, above the transition, shows no field dependence, as expected. As in the case of Sr_3NiRhO_6 and Sr_3NiIrO_6, the magnetic data of Sr_3CuRhO_6 look very similar to those of the iridium analogue, Sr_3CuIrO_6 (25).

The data for the incommensurate phases are shown in Fig. 10, for both $Sr_3NiRhO_{6+\delta}$ and $Sr_3CuRhO_{6+\delta}$. It is important to point out the complete absence of any features in the susceptibility of the incommensurate phases. Between 2 and 300 K there is no sign of any magnetic transition, and the ZFC and FC data overlay.

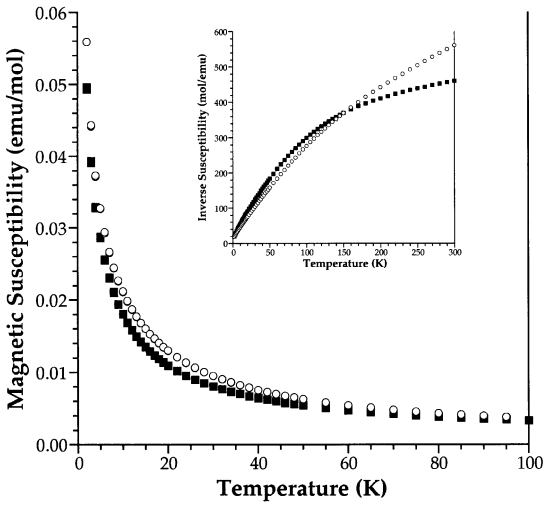

FIG. 10. Temperature dependence of the ZFC and FC magnetic susceptibility measured at 5 kG for incommensurate $Sr_3NiRhO_{6+\delta}$ (■) and $Sr_3CuRhO_{6+\delta}$ (○). Inset: Temperature dependence of the inverse susceptibility measured at 5 kG for incommensurate $Sr_3NiRhO_{6+\delta}$ (■) and $Sr_3CuRhO_{6+\delta}$ (○).

DISCUSSION

Structures

The Rietveld refinements of Sr_3NiRhO_6 and Sr_3CuRhO_6 are shown in Figs. 2 and 3. The fit of the diffraction data to the known $m = 0$, $n = 1$ structure of the $A_{3n+3m}A'_nB_{3m+n}O_{9m+6n}$ family is reasonable, although adversely affected by the presence of the incommensurate phase, and confirms the structural model for these materials. The presence of the incommensurate phase worsens the fit, but not unduly so. Unlike the iridium analogues, Sr_3NiIrO_6 and Sr_3CuIrO_6, which readily form and show no signs of transforming into an incommensurate phase, even when heated in excess of 1300°C, the two rhodates have a strong tendency to pick up oxygen during the synthesis and to transform into incommensurate modifications that no longer resemble the simple $m = 0$, $n = 1$ structure. A similar tendency has been observed for other Sr–Rh–O phases (37) and in Sr_3ZnRhO_6 (1). The processes involved in the transformation between a commensurate and an incommensurate phases are not well understood; however, there are several processes that are believed to participate in the transformation (39). One is the incorporation of extra oxygen into a trigonal prismatic site, resulting in the conversion of one trigonal prismatic site into two octahedral sites, giving rise to a net gain in oxygen for the material. Another potential process involves the migration of $[A]_\infty$ chain cations into the transition metal $[(A', B)O_3]_\infty$ chain. One can speculate that the degree of incommensurability that can be achieved by oxygen uptake is limited by the maximum oxidation state that the metals in the $[(A', B)O_3]_\infty$ chain can take on: in the case of nickel $+3$ to $+4$, in the case of copper $+3$, and in the case of rhodium $+4$ to $+5$. In the limit we achieve the $BaNiO_3$ structure type, which consists of all face-shared octahedra, with an average oxidation state of $+4$ in the $[(A', B)O_3]_\infty$ chain. It is possible that some of these materials are capable of forming an essentially infinite number of incommensurate structures with a continually adjustable c_1/c_2 ratio. However, some compositions clearly prefer quite specific c_1/c_2 ratios, for example, Sr_3NiPtO_6 or Sr_3PbNiO_6, suggesting that perhaps specific cation and anion radius ratios might favor specific compositions and, hence, structures. As more incommensurate structures are thoroughly structurally characterized, it might be possible to substantiate such a trend.

Figures 5 and 6 show the indexed XRD pattern for the incommensurate phases of $Sr_3NiRhO_{6+\delta}$ and $Sr_3CuRhO_{6+\delta}$, where the peaks associated with the two subsystems and those of the modulated structure are marked. Several examples of related structures are known (1, 12, 13, 39). The composition is directly related to the γ value by the relationship $\gamma = (1 + x)/2$ where $\gamma = c_1/c_2$ (11, 13). Therefore, determination of the c_1/c_2 ratio is sufficient to determine the composition and hence the polyhedral chain sequence (11). The ratios of $c_1/c_2 = 0.6716$ and 0.6824 for the nickel and copper phases, respectively, are considerably less than the ideal ratio of 3/4 predicted for the commensurate phase, Sr_3MRhO_6. These c_1/c_2 ratios can be roughly approximated (using the Farey tree) to a value of $x = p/q = 1/3$ (11). Such a value of x corresponds to an average structure of two octahedra to one trigonal prism along the chain direction. TGA data showing increased oxygen content, as compared to the commensurate analogues, supports the conversion of trigonal prisms to octahedra. The increased number of coordination sites within the polyhedra chain necessitate metal vacancies or incorporation of $[A]_\infty$ cations. At this point, neither model can be confirmed as further structural characterization needs to be pursued.

As demonstrated, we were able to synthesize the Sr_3MRhO_6 (M = Cu, Ni) members of this structural family; however, the compounds are very sensitive to specific synthetic conditions (oxygen partial pressure, heating rate, temperature, time, precursors, etc.) as shown by the growth of the incommensurate phase. Hence each compound (commensurate and incommensurate) could be considered a unique composition with a unique structure and concomitant properties.

Magnetic Properties

In the absence of magnetic neutron data, it is impossible to make definitive statements concerning the magnetic structure in these materials. While it is certainly possible to carry out such measurements, based on the fact that many

of the magnetic measurements display a distinct difference between the ZFC and FC data, one might suspect that no long-range order detectable by neutrons exists in the nickel and copper rhodates. The magnetic susceptibility of Sr_3NiRhO_6 looks almost identical to that of Sr_3NiIrO_6, except for the difference in the magnetic transition temperatures of 15 and 25 K, respectively. Low-temperature neutron diffraction experiments in Sr_3NiIrO_6 did not result in the observation of any magnetic peaks (25) and, consequently, none might be expected for the rhodate analogue. Sr_3NiRhO_6 has two unpaired electrons on the trigonal prismatic Ni^{2+} and one unpaired electron on the octahedrally coordinated Rh^{4+} that can couple magnetically with each other. It is not unexpected, therefore, to find complex magnetic behavior in this material. The sharp drop in the susceptibility for the ZFC data contrasts with the lack of a drop for the FC data. This striking difference between FC and ZFC is characteristic of a system exhibiting geometric frustration or spin glass behavior, arising from the pseudo triangular chain arrangement found in these materials. An antiferromagnetic interaction between the chains would lead to spin frustration, a situation where under ZFC conditions a low-energy spin arrangement forms. Under FC conditions, however, a higher energy spin arrangement forms, as observed in the magnetic data.

The magnetic interactions in Sr_3CuRhO_6, with one unpaired electron each on the Cu^{2+} and the Rh^{4+}, follow a similar pattern, in that the ZFC and FC data do not overlay. Recently, Beauchamp and co-workers (40) carried out an investigation on the magnetic properties of Sr_3CuIrO_6, and found evidence for a 2D ferromagnetic xy interaction in this material. This magnetic order is consistent with the temperature dependence of the susceptibility at low temperatures, and is followed by a 3D magnetic transition below about 20 K. In addition, Sampathkumaran and co-workers recently investigated the $Sr_3Cu_{1-x}Zn_xIrO_6$ system and, based on AC susceptibility measurements, concluded that Sr_3CuIrO_6 exhibits spin glass behavior in zero field, but is driven toward a ferromagnetic state with reduced moment by the application of an applied field (41, 42). Fig. 9, a field sweep measured at 3K, is consistent with such a ferromagnetic state.

In contrast to the magnetic data of the commensurate phases, the magnetic susceptibility data for the incommensurate nickel and copper phases are featureless, however, they do not give a reasonable fit to Curie–Weiss behavior due to the nonlinearity of the inverse susceptibility plot. The difference in the magnetic data can be attributed to several factors. For example, rather than having a chain containing magnetic cations in every coordination site, there are now vacancies present in the chain. Furthermore, the average oxidation states of the metals in the chain have increased and, due to the incommensurate relationship between the $[A]_\infty$ and $[(A',B)O_3]_\infty$ chains, the superexchange pathways responsible for magnetic order are potentially disrupted. All of these possibilities could explain the lack of any features in the susceptibility data.

The incommensurate nature of these structures appears to result from the transformation of trigonal prisms into octahedra, as shown by the lower than ideal c_1/c_2 ratio and the increased oxygen content for these materials. Therefore, the potential vacancies within the $[(A',B)O_3]_\infty$ chain, also, could disrupt the magnetic coupling. While one cannot generalize to other structural members of this family or identical structures with different metals, one should nonetheless bear in mind that the presence of an irrational c_1/c_2 ratio probably does not favor long-range magnetic order.

ACKNOWLEDGMENTS

Funding for this research was provided by the National Science Foundation through Grant DMR: 9873570. Research carried out in part at the National Synchrotron Light Source, Brookhaven National Laboratory, which is supported by the U.S. Department of Energy, Division of Materials Science and Division of Chemical Sciences.

REFERENCES

1. R. C. Layland and H.-C. zur Loye, *J. Alloys Compd.* **299,** 118 (2000).
2. P. Núñez, M. A. Rzeznik, and H.-C. zur Loye, *Z. Anorg. Allg. Chem.* **623,** 1269 (1997).
3. R. C. Layland, S. L. Kirkland, P. Núñez, and H.-C. zur Loye, *J. Solid State Chem.* **139,** 416 (1998).
4. J. B. Claridge, R. C. Layland, R. D. Adams, and H.-C. zur Loye, *Z. Anorg. Allg. Chem.* **623,** 1131 (1997).
5. T. N. Nguyen and H.-C. zur Loye, *in* "Neutron Scattering in Materials Science" (D. A. Neumann, T. P. Russel, and B. J. Wuensch, Eds.), Vol. 376, p. 603. MRS Symposia Proceedings, 1995.
6. M. D. Smith, J. K. Stalick, and H.-C. zur Loye, *Chem. Mater.* **11,** 2984 (1999).
7. J. B. Claridge and H.-C. zur Loye, *Chem. Mater.* **10,** 2320 (1998).
8. K. E. Stitzer, A. El Abed, J. Darriet, and H.-C. zur Loye, *J. Am. Chem. Soc.* **123,** 8790 (2001).
9. K. E. Stitzer, J. Darriet, and H.-C. zur Loye, *Curr. Opin. Solid State Mater. Sci.*, in print.
10. J. Darriet and M. A. Subramanian, *J. Mater. Chem.* **5,** 543 (1995).
11. J. M. Perez-Mato, M. Zakhour-Nakhl, F. Weill, and J. Darriet, *J. Mater. Chem.* **9,** 2795 (1999).
12. M. Zakhour-Nakhl, J. B. Claridge, J. Darriet, F. Weill, H.-C. zur Loye, and J. M. Perez-Mato, *J. Am. Chem. Soc.* **122,** 1618 (2000).
13. M. Evain, F. Boucher, O. Gourdon, V. Petricek, M. Dusek, and P. Bezdicka, *Chem. Mater.* **10,** 3068 (1998).
14. K. Ukei, A. Yamamoto, Y. Watanabe, T. Shishido, and T. Fukuda, *Acta Crystallogr Sect. B* **49,** 67 (1993).
15. M. Zakhour-Nakhl, F. Weill, J. Darriet, and J. M. Perez-Mato, *Inter. J. Inorg. Mater.* **2,** 71 (2000).
16. P. D. Battle, G. R. Blake, J. Darriet, J. G. Gore, and F. Weill, *J. Mater. Chem.* **7,** 1559 (1997).
17. M. Onoda, M. Saeki, A. Yamamoto, and K. Kato, *Acta Crystallogr. Sect. B* **49,** 929 (1993).
18. P. D. Battle, G. R. Blake, J. Sloan, and J. F. Vente, *J. Solid State Chem.* **136,** 103 (1998).
19. M. Zakhour-Nakhl, J. Darriet, J. B. Claridge, H.-C. zur Loye, and J. M. Perez-Mato, *Inter. J. Inorg. Mater.* **2,** 503 (2000).

20. J. B. Claridge, R. C. Layland, W. H. Henley, and H.-C. zur Loye, *Chem. Mater.* **11,** 1376 (1999).
21. K. S. Lee, H. J. Koo, and M. H. Whangbo, *Inorg. Chem.* **38,** 2199 (1999).
22. A. P. Ramirez, *Annu. Rev. Mater. Sci.* **24,** 453 (1994).
23. H. Kageyama, K. Yoshimura, and K. Kosuge, *J. Solid State Chem.* **140,** 14 (1998).
24. S. Kawasaki, M. Takano, and T. Inami, *J. Solid State Chem.* **145,** 302 (1999).
25. T. N. Nguyen and H.-C. zur Loye, *J. Solid State Chem.* **117,** 300 (1995).
26. S. Niitaka, H. Kageyama, M. Kato, K. Yoshimura, and K. Kosuge, *J. Solid State Chem.* **146,** 137 (1999).
27. H. Fjellvåg, E. Gulbrandsen, S. Aasland, A. Olsen, and B. C. Hauback, *J. Solid State Chem.* **124,** 190 (1996).
28. S. Aasland, H. Fjellvåg, and B. Hauback, *Solid State Commun.* **101,** 187 (1997).
29. H. Kageyama, K. Yoshimura, K. Kosuge, M. Azuma, M. Takano, H. Mitamura, and T. Goto, *J. Phys. Soc. Jpn.* **66,** 3996 (1997).
30. H. Kageyama, K. Yoshimura, K. Kosuge, H. Mitamura, and T. Goto, *J. Phys. Soc. Jpn.* **66,** 1607 (1997).
31. H. Kageyama, K. Yoshimura, K. Kosuge, X. Xu, and S. Kawano, *J. Phys. Soc. Jpn.* **67,** 357 (1998).
32. A. Maignan, C. Michel, A. C. Masset, C. Martin, and B. Raveau, *Eur. Phys. J. B* **15,** 657 (2000).
33. T. N. Nguyen, D. M. Giaquinta, and H.-C. zur Loye, *Chem. Mater.* **6,** 1642 (1994).
34. A. P. Wilkinson, A. K. Cheetham, W. Kunnman, and Å. Kvick, *Eur. J. Solid State Inorg. Chem.* **28,** 453 (1991).
35. H. M. Rietveld, *J. Appl. Crystallogr.* **2,** 65 (1969).
36. A. C. Larson and R. B. Von Dreele, "General Structure Analysis System (GSAS)." Los Alamos National Laboratory Report LA-UR-86-748, 1994.
37. J. B. Claridge and H.-C. zur Loye, *in* "Solid-State Chemistry of Inorganic Materials II" (S. M. Kauzlarich, G. McCarron, A. W. Sleight, and H.-C. zur Loye, Eds.), Vol. 547, p. 183. MRS Symposia Proceedings, 1999.
38. G. R. Blake, J. Sloan, J. F. Vente, and P. D. Battle, *Chem. Mater.* **10,** 3536 (1998).
39. M. Huvé, C. Renard, F. Abraham, G. Van Tendeloo, and S. Amelinckx, *J. Solid State Chem.* **135,** 1 (1998).
40. S. H. Irons, T. D. Sangrey, K. M. Beauchamp, M. D. Smith, and H.-C. zur Loye, *Phys. Rev. B* **61,** 11594 (2000).
41. A. Niazi, E. V. Sampathkumaran, P. L. Paulose, D. Eckert, A. Handstein, and K.-H. Müller, arXiv.org e-Print archive, available at http://xxx.lanl.gov, cond-mat/0107159 (2001).
42. A. Niazi, E. V. Sampathkumaran, P. L. Paulose, D. Eckert, A. Handstein, and K.-H. Müller, arXiv.org e-Print archive, available at http://xxx.lanl.gov, cond-mat/0107069 (2001).